EPJ manuscript No.
(will be inserted by the editor)

Motion and mixing for multiple ferromagnetic microswimmers

Andrew D. Gilbert, Feodor Y. Ogrin, Peter G. Petrov, and C. Peter Winlove

College of Engineering, Mathematics and Physical Sciences,
University of Exeter, Exeter, U.K.

Received: date / Revised version: date

Abstract. This paper concerns the interaction of several ferromagnetic microswimmers, their motion and the resulting fluid mixing. Each swimmer consists of two ferromagnetic beads joined by an elastic link, and is driven by an external, time-dependent magnetic field. The external field provides a torque on a swimmer and, together with the varying attraction between the magnetic beads, generates a time-irreversible motion leading to persistent swimming in a low Reynolds number environment.
The aim of the present paper is to consider the interactions between several swimmers. A regime is considered in which identical swimmers move in the same overall direction, and their motion is synchronised because of driving by the external field. It is found that two swimmers tend to encircle one another while three undergo more complicated motion that may involve the braiding of swimmer trajectories. By means of approximations it is established that the interaction between pairs of swimmers gives circulatory motion which falls off with an inverse square law and is linked to their overall speed of motion through the fluid. As groups of two or more swimmers move through the fluid they process fluid, leaving behind a trail of fluid that has undergone mixing: this is investigated by following streak lines numerically.

PACS. 47.63.Gd swimming microorganisms – 47.61.Ne micromixing – 47.63.mf low-Reynolds-number motions

There is a long history of the study of how living organisms can propel themselves through a fluid by means of changes of shape of their boundaries, both in low and in high Reynolds number regimes [1]–[5]. Recently there has been much interest in fabricating microscale swimmers and related devices, aimed at potential application for targetted drug delivery or for pumping or mixing in microfluidic devices. Models studied include those based on three spherical beads [6]–[8], chains of magnetic beads coupled by flexible links [9]–[13], and paramagnetic colloidal particles in the presence of a boundary [14]. Magnetic driving has also been used to generate motion in arrays of artificial cilia, and so to pump and mix fluid on microscales [15–17].

One recent model swimmer proposed consists of two ferromagnetic particles or 'beads' joined by an elastic element forming a dumb-bell [18]–[21], and driven by an external time-dependent magnetic field. The particles are magnetically anisotropic and their magnetic fields are affected by the external field. This leads to a time-varying dipole force between them, and so a relative radial motion. At the same time there is a time-dependent torque from the external field causing an oscillatory rotational motion of the dumb-bell. In appropriate regimes the motion of the swimmer fails to be time-reversible, a necessary condition for swimming at low Reynolds number [22], and the swimmer duly moves through the fluid. In the paper [21] the mechanisms for persistent swimming were studied by means of theoretical models and small-scale simulations, and a general discussion of driven multi-bead swimmers may be found in [23]–[25]. There are many advantages in both driving and controlling a fabricated swimmer by means of externally applied magnetic fields and exploiting the ferromagnetic properties of the beads. In the limit of a colloidal suspension of many, many beads on nanoscales, a so-called ferrofluid is obtained and complex fluid motions and instabilities can be driven magnetically [26].

The present paper extends the study [21] to consider the motion of several, identical swimmers. Each swimmer consists of two ferromagnetic beads joined by an elastic link. In the simplest model, one bead, the larger, is magnetically 'soft' and so its field direction follows the external field. The other bead, the smaller one, is magnetically 'hard', and so has a fixed magnetic field. In isolation and with appropriate parameter values each swimmer moves in the same direction with a given velocity. Our interest is now to understand how several such swimmers interact. Do they attract or repel, and how do the interactions fall off with distance? Do they lead to complex motions, and how do they mix passive scalars in the fluid? We investigate this by means of numerical simulations, supported by approximations. There have been a number of recent stud-

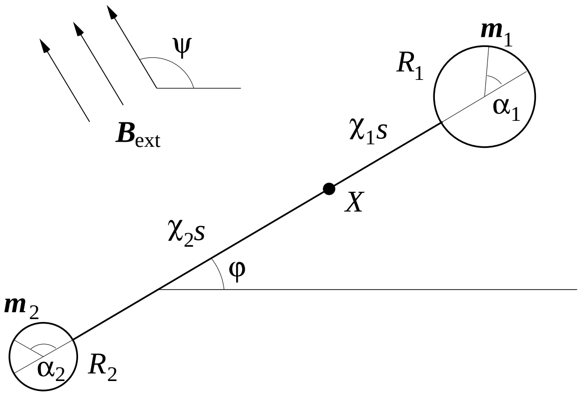

Fig. 1. Geometry of a swimmer.

ies of the motion of pairs of interacting three-sphere and dumb-bell swimmers [27]–[32] and we give comments and comparison in our final discussion section. For the present we simply note that since our swimmers are identical and externally driven, they are naturally synchronised, and so their behaviour may well differ from that of autonomous organisms in biological systems.

1 Governing equations with fluid interactions

The basic geometry of a single swimmer is shown in figure 1. The swimmer is defined by the distance s between the two beads, the angle ϕ to some axis and the position $\boldsymbol{X}$ of its centre of reaction, which is the average of the two bead positions weighted by their radii R_1 and R_2 [33]. Note that we assume the swimmer beads are spherical and are surrounded by fluid in three dimensions; however we take the swimmers to be confined to a plane. In current experiments (not reported here), swimmers sit at a fluid–air interface. In dimensional quantities the leading order equations governing the degrees of freedom (s, ϕ) are

$$6\pi\eta(\chi_1^2 R_1 + \chi_2^2 R_2)\dot{s} + k(s - l_0) = \frac{3\mu_0 m_1 m_2}{4\pi s^4}\left[\cos(\alpha_2 - \alpha_1) - 3\cos\alpha_1\cos\alpha_2\right], \tag{1}$$

$$6\pi\eta(\chi_1^2 R_1 + \chi_2^2 R_2)s^2\dot{\phi} = -B_{\rm ext} b[m_1\sin(\phi + \alpha_1 - \psi) + m_2\sin(\phi + \alpha_2 - \psi)]. \tag{2}$$

Here the fluid inertia is neglected: we are working in a Stokes regime where the Reynolds number is effectively zero. The fluid viscosity is η, k is a spring constant and l_0 the natural length for the elastic element joining the two beads. The constants $\chi_1 = R_2/(R_1 + R_2)$, $\chi_2 = R_1/(R_1 + R_2)$ are simply weights. In these equations we can identify the viscous drag terms (first terms in (1, 2)), the elastic restoring force (second term in (1)), the magnetic attraction of the beads (right-hand side of (1)), and the magnetic torque on the system (right-hand side of (2)). $B_{\rm ext}$ and ψ are the magnitude and direction of the external field and other equations have to be included to specify the time-dependence of the angles α_1 and α_2 giving the field directions of the two magnetic beads, as discussed in [21]. The equations above give the time dependence of (s, ϕ) with purely Stokes drag on each bead. With only these terms, the centre of reaction $\boldsymbol{X}$ is fixed in space [33] and there cannot be persistent motion, that is swimming. To give motion of an individual swimmer we need to include the leading order viscous interaction between the moving spherical beads in the system [19,33], resulting in an equation for the centre of reaction $\boldsymbol{X}$,

$$6\pi\eta(R_1 + R_2)\dot{\boldsymbol{X}} = -\frac{9\pi}{2}\frac{\eta R_1 R_2}{s}(\chi_2 - \chi_1)(2\dot{s}\hat{\boldsymbol{r}} + s\dot{\phi}\hat{\boldsymbol{\phi}}). \tag{3}$$

Here $\hat{\boldsymbol{r}}$ is a unit vector from bead 2 to bead 1 and $\hat{\boldsymbol{\phi}}$ is a perpendicular unit vector.

For magnetic properties, in this paper we take the simplest *soft–hard system* used in [21], in which bead 1 is magnetically completely soft, and so its magnetic field direction $\boldsymbol{m}_1$ follows that of the externally imposed magnetic field $\boldsymbol{b}(t)$, with the angle $\alpha_1 = \psi - \phi$ in figure 1. Bead 2 however is magnetically entirely hard and its field direction $\boldsymbol{m}_2$ is fixed, say along the axis of the swimmer, with direction $\alpha_2 = 0$.

In dimensionless variables the degrees of freedom (s, ϕ) are then governed by the *internal dynamics*,

$$\varpi\dot{s} + s - 1 = -2A_{\rm mag}s^{-4}\cos(\psi - \phi), \tag{4}$$

$$\varpi s^2\dot{\phi} = A_{\rm ext}\sigma^{-1}b\sin(\psi - \phi), \tag{5}$$

where the time-dependent external magnetic field is given by

$$\boldsymbol{b} \equiv b(\cos\psi, \sin\psi) = (\alpha\cos t, \beta\sin t), \tag{6}$$

with α and β constant. For a complete discussion of the non-dimensionalisation, we refer the reader to [21]. Here we simply note that it is based on the length scale $\mathcal{L}$ as the swimmer bead separation l_0, time scale $\mathcal{T} = \omega^{-1}$, the inverse of the frequency of the magnetic field, and mass scale $\mathcal{M} = k\omega^{-2}$ where k is the spring constant of the elastic link. In these terms $A_{\rm mag}$ is a dimensionless measure of the dipole attraction between the two magnets, which varies as the soft magnetic dipole direction follows the external field. The term involving $A_{\rm ext}$ gives the torque on the hard bead from the external field, and those involving ϖ give the dimensionless magnitude of the viscous drag. The constant $\sigma^2 = m_1/m_2$ is the ratio of the magnetisations m_j of the two beads.

Below we will also need the geometrical constants $\rho^2 = R_1/R_2$ and the small parameter $\varepsilon^2 = R_1R_2/l_0^2 \ll 1$ used in the expansions of [21]. This controls the overall swimming velocity given by the non-dimensional form of (3), namely

$$(\rho + \rho^{-1})\boldsymbol{X} = -\frac{3\varepsilon}{4}(\chi_2 - \chi_1)\int_0^t s^{-1}(2\dot{s}\hat{\boldsymbol{r}} + s\dot{\phi}\hat{\boldsymbol{\phi}})\,dt. \tag{7}$$

The values used in the present paper and [21] are

$$A_{\rm mag} = 0.0403, \quad A_{\rm ext} = 0.207, \quad \varpi = 0.0503, \tag{8}$$

$$\sigma = 2\sqrt{2}, \quad \rho = \sqrt{2}, \quad \varepsilon = 2^{-5/2}, \quad (\alpha, \beta) = (1, 0.02). \tag{9}$$

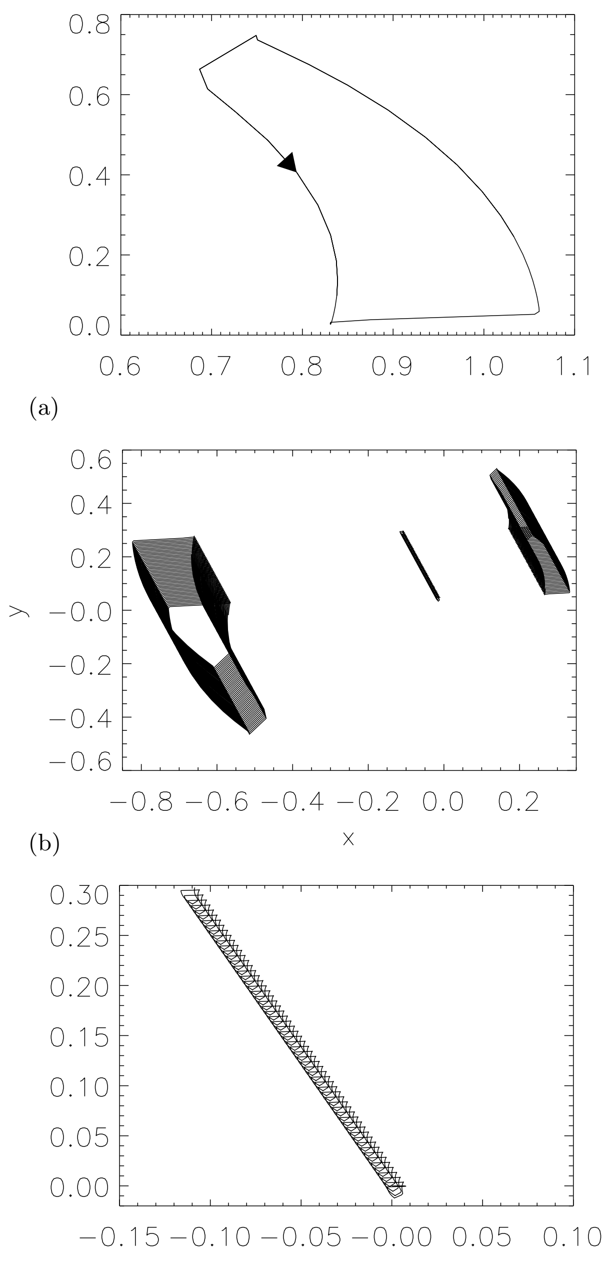

Fig. 2. Dynamics and motion of a single swimmer. (a) shows a limit cycle in a phase plane with s and ϕ as polar coordinates. In (b) is plotted the paths of the two beads and, in the middle, the centre of reaction $\boldsymbol{X}(t)$, while (c) again shows $\boldsymbol{X}(t)$.

Before introducing multiple swimmers, we illustrate the motion of a single swimmer with these parameter values in figure 2, with panels taken from figure 3 of [21]. Panel 2(a) shows the solution of the ODEs in equations (4,5) as a limit cycle in a phase plane with (s, ϕ) as polar coordinates. The arrow indicates the sense of increasing time for the internal dynamics. To obtain the overall motion, equation (7) is integrated, and panel 2(b) shows the paths of the two beads, the small one to the left and the large one to the right, with the path $\boldsymbol{X}(t)$ of the centre of reaction in between. There is systematic swimming motion which arises through fluid interactions, in the direction of increasing y and decreasing x and this is shown in more detail in panel 2(c). Note that there are essentially two time-scales involved here: the fast ‘rocking’ motion of the beads from the internal dynamics in panel (a), and the slow, persistent swimming evident in panel (c).

We will now consider a set of identical swimmers in the fluid, given by coordinates $(s_j, \phi_j, \boldsymbol{X}_j)$. Each swimmer has soft and hard beads with positions

$$\boldsymbol{r}_{1j} = \boldsymbol{X}_j + \chi_1 s_j \hat{\boldsymbol{r}}_j, \quad \boldsymbol{r}_{2j} = \boldsymbol{X}_j - \chi_2 s_j \hat{\boldsymbol{r}}_j. \tag{10}$$

The velocities of the beads are denoted $\dot{\boldsymbol{r}}_{1j}$ and $\dot{\boldsymbol{r}}_{2j}$, and it is also useful to define the leading order velocities resulting only from the internal dynamics as

$$\boldsymbol{v}_{1j} = \chi_1(\dot{s}_j \hat{\boldsymbol{r}}_j + s_j \dot{\phi}_j \hat{\boldsymbol{\phi}}_j), \quad \boldsymbol{v}_{2j} = -\chi_2(\dot{s}_j \hat{\boldsymbol{r}}_j + s_j \dot{\phi}_j \hat{\boldsymbol{\phi}}_j), \tag{11}$$

these neglecting the order-ϵ motions of the centres of reaction.

If we temporarily revert to dimensional quantities (with η the fluid viscosity), the total viscous force on bead 1 of swimmer j from all the other beads is approximately

$$\begin{aligned} \boldsymbol{F}_{1j} = {} & -6\pi\eta R_1 \dot{\boldsymbol{r}}_{1j} + \frac{9\pi}{2}\frac{\eta R_1 R_2}{s_j}(\hat{\boldsymbol{r}}_j \hat{\boldsymbol{r}}_j + \boldsymbol{I}) \cdot \boldsymbol{v}_{2j} \\ & + \sum_i \frac{9\pi}{2}\frac{\eta R_1 R_1}{s_{1j1i}}(\hat{\boldsymbol{r}}_{1j1i}\hat{\boldsymbol{r}}_{1j1i} + \boldsymbol{I}) \cdot \boldsymbol{v}_{1i} \\ & + \sum_i \frac{9\pi}{2}\frac{\eta R_1 R_2}{s_{1j2i}}(\hat{\boldsymbol{r}}_{1j2i}\hat{\boldsymbol{r}}_{1j2i} + \boldsymbol{I}) \cdot \boldsymbol{v}_{2i} \end{aligned} \tag{12}$$

and likewise for bead 2 of swimmer j with interchange of indices 1 and 2. The leading term gives the Stokes drag, followed by the leading order interaction with the other bead of the same swimmer, and then with the two beads of the other swimmers. Here

$$\boldsymbol{r}_{1j1i} = \boldsymbol{r}_{1j} - \boldsymbol{r}_{1i}, \quad s_{1j1i} = |\boldsymbol{r}_{1j1i}|, \tag{13}$$

etc., and $\boldsymbol{I}$ is the identity matrix.

We obtain the equation of motion for the centre of reaction of the jth swimmer by setting $\boldsymbol{F}_{1j} + \boldsymbol{F}_{2j} = 0$. In non-dimensional terms this amounts to

$$\begin{aligned} (\rho + \rho^{-1})\dot{\boldsymbol{X}}_j = {} & -\frac{3\varepsilon}{4}(\chi_2 - \chi_1) s_j^{-1}(2\dot{s}_j \hat{\boldsymbol{r}}_j + s_j \dot{\phi}_j \hat{\boldsymbol{\phi}}_j) \\ & + \frac{3\varepsilon}{4}\sum_{i \neq j} \boldsymbol{K}_{ji} \cdot (\dot{s}_i \hat{\boldsymbol{r}}_i + s_i \dot{\phi}_i \hat{\boldsymbol{\phi}}_i), \end{aligned} \tag{14}$$

where the interaction tensors $\boldsymbol{K}_{ji}$ are given by

$$\begin{aligned} \boldsymbol{K}_{ji} = {} & \frac{\chi_2}{s_{1j1i}}(\hat{\boldsymbol{r}}_{1j1i}\hat{\boldsymbol{r}}_{1j1i} + \boldsymbol{I}) - \frac{\chi_2}{s_{1j2i}}(\hat{\boldsymbol{r}}_{1j2i}\hat{\boldsymbol{r}}_{1j2i} + \boldsymbol{I}) \\ & + \frac{\chi_1}{s_{2j1i}}(\hat{\boldsymbol{r}}_{2j1i}\hat{\boldsymbol{r}}_{2j1i} + \boldsymbol{I}) - \frac{\chi_1}{s_{2j2i}}(\hat{\boldsymbol{r}}_{2j2i}\hat{\boldsymbol{r}}_{2j2i} + \boldsymbol{I}). \end{aligned} \tag{15}$$

The first term on the right-hand side of (14) is the fluid interaction in a single swimmer driving its motion as in (7), while the sum over the remaining terms gives the interaction between different swimmers.[1]

Some notes are in order: our focus is on the overall motion of the swimmers, which means the leading order evolution of the centres of reaction $\boldsymbol{X}_j$, at order ε in our non-dimensionalisation. Fluid interactions will also lead to source terms in the equations (4,5) giving the internal dynamics (s_j, ϕ_j): however these will give uninteresting corrections of order ε, and so even smaller corrections to the $\boldsymbol{X}_j$ motion of order ε^2. For the same reason when we use the velocities (11) for the beads, we are neglecting the contribution of $\dot{\boldsymbol{X}}_j$ which will again give order ε^2 corrections to $\dot{\boldsymbol{X}}_j$ in (14). Our experience with simulations confirms that such corrections are unimportant and so we aim for the cleanest system in which only leading order terms are retained in the equations for the internal dynamics (4,5) (for each (s_j, ϕ_j)) and for the centres of reaction (14,15).

2 Simulations of the full dynamics

We have run simulations of small numbers of swimmers. With the same initial conditions the internal dynamics of the swimmers are identical, with $s = s_j$ and $\phi = \phi_j$, say. For the soft–hard system the internal degrees of freedom rapidly settle to a limit cycle in (s, ϕ) phase space, seen in figure 2(a). Figure 3(a) shows the motion of two swimmers $j = 1, 2$, initially placed at

$$\boldsymbol{X}_j|_{t=0} = (3j - 3, 0). \tag{16}$$

For each swimmer, the solid curves show the motion of the two beads and the centre of reaction. These are plotted every period of the internal dynamics, so the details of the motion are absent. The two swimmers travel in the same direction and also circulate about each other, maintaining an approximately constant separation. Note that horizontal and vertical scales differ here and elsewhere.

The behaviour of three or more swimmers is more complicated. Figures 3(b) and (c) show the motions of three and four swimmers initially placed according to (16). Visible are periods in which two swimmer 'partners' circle about each other, with occasional interchange of partners occurring in the case of three swimmers. To confirm this figure 3(d) shows the relative displacements $\boldsymbol{X}_3 - \boldsymbol{X}_2$ (solid) and $\boldsymbol{X}_2 - \boldsymbol{X}_1$ (dotted) in the case of three swimmers, for a longer run. We observe here that there are periods when swimmers 3 and 2 circulate about each other, or swimmers 1 and 2, at a distance of approximately 2 units.

[1] Note we have not included magnetic interactions between different swimmers, on account of their rapid, r^{-4} fall-off. We have also neglected the r^{-3} component of the viscous interaction (cf. (25) below) as we recover a dominant inverse square law on large scales, making the approximations used uniform for $\varepsilon \ll 1$ and $r \gg 1$.

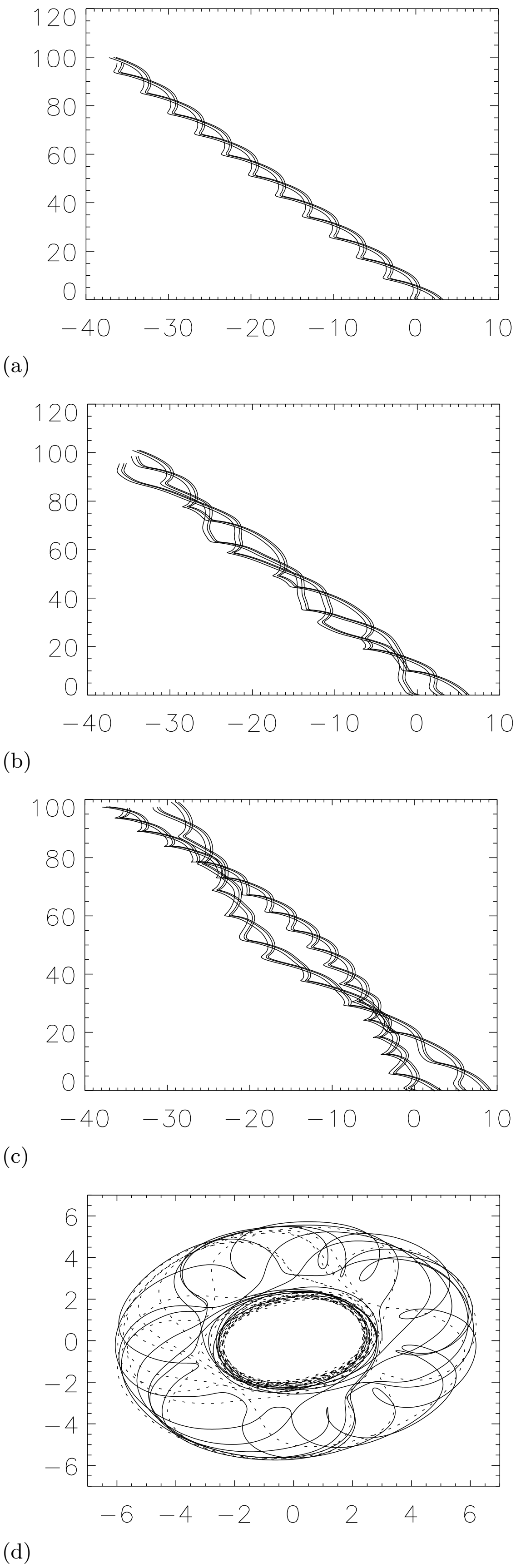

Fig. 3. Motion of (a) two (b) three and (c) four swimmers for $N = 2 \times 10^4$ cycles, and (d) relative displacements for three swimmers in (b) but for $N = 10^5$ cycles, showing $\boldsymbol{X}_3 - \boldsymbol{X}_2$ (solid) and $\boldsymbol{X}_2 - \boldsymbol{X}_1$ (dotted).

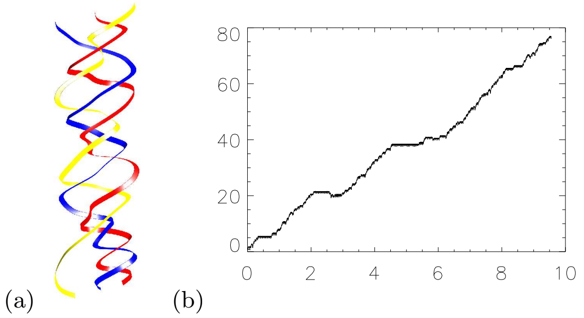

(a) (b)

Fig. 4. Motion of three swimmers: (a) shows the braid generated for $N = 2 \times 10^4$ cycles and (b) the growth in $\log L(t)$ plotted against $t/10^6$ over $N = 2 \times 10^6$ cycles.

The fact that pairs of swimmers remain relatively well-separated is useful confirmation of the validity of the far-field approximations used, at least at a qualitative level, and is further explored below. For large numbers of swimmers, say five or six, collisions tend to occur after some time (not shown), and the model ceases to have any validity.

The motion of three swimmers is sufficiently complicated that their trajectories define a braid. Figure 4 depicts the positions $\boldsymbol{X}_j(t)$ plotted in (X, Y, t) space with t as the 'vertical coordinate' and with the overall velocity of the group removed. Swimmer $j = 1$ is yellow, 2 is blue and 3 is red, and their paths in this space–time diagram give strings that braid and tangle as time increases. This braiding is associated with stretching of material lines in the fluid around the swimmers and so with mixing in the fluid flow [34]. Figure 4(b) quantifies the braiding over a longer time period as measured by taking a notional material loop in the fluid surrounding swimmers 1 and 2: as the braiding occurs, the length of the loop must increase and we measure its length $L(t)$ as a function of time, using the method of [35].[2](There is a similar, dotted line for a loop encircling swimmers 2 and 3, but this is less visible). We observe clear overall exponential growth (but some fluctuations) at a rate $h \simeq 8 \times 10^{-6}$. This is a topological measure of the line-stretching in the flow, in other words, how much stretching is guaranteed only from the braiding of the swimmer positions in space-time. The *actual* exponential growth rate of material curves in the flow (measured in two dimensions by the so-called topological entropy) will generally be greater than this lower bound [34]. In this system the braiding is capturing the line-stretching and mixing on the slow time-scale of swimmer motion seen in figure 3 but is likely to be enhanced by the rocking motion of the swimmers on the fast time-scale, as shown in figure 2.

[2] We follow [35] in our measurements, except that we define the length as $L = \sum_j \nu_j$, to use the notation of figure 9 of that paper. In the case of $n = 3$ swimmers, as here, $L = 4|a_1| + 2|b_1|$.

3 Approximate swimmer motion

The relative simplicity of the motion of two and three swimmers suggests seeking an approximation which takes a further step of averaging over a cycle of the internal dynamics. We develop this in the present section. With all the swimmers swimming in synchrony we have $s = s_j$, $\phi = \phi_j$ and the vector joining the pair of beads in each swimmer is the same, namely

$$\boldsymbol{r} = s\hat{\boldsymbol{r}} = \boldsymbol{r}_{1j} - \boldsymbol{r}_{2j}, \quad \dot{\boldsymbol{r}} = \dot{s}\hat{\boldsymbol{r}} + s\dot{\phi}\hat{\boldsymbol{\phi}}. \tag{17}$$

Given this, we have

$$\boldsymbol{r}_{1j1i} = \boldsymbol{r}_{2j2i} = \boldsymbol{X}_{ji}, \quad \boldsymbol{r}_{2j1i} = \boldsymbol{X}_{ji} - \boldsymbol{r}, \quad \boldsymbol{r}_{1j2i} = \boldsymbol{X}_{ji} + \boldsymbol{r}, \tag{18}$$

with $\boldsymbol{X}_{ji} = \boldsymbol{X}_j - \boldsymbol{X}_i$. We may now expand $\boldsymbol{K}_{ji}$ in a Taylor series, assuming that $|\boldsymbol{r}| \ll X_{ji} = |\boldsymbol{X}_{ji}|$. The leading order terms, in X_{ji}^{-1}, vanish to leave

$$\boldsymbol{K}_{ji} = -\frac{\boldsymbol{r}\boldsymbol{X}_{ji} + \boldsymbol{X}_{ji}\boldsymbol{r}}{X_{ji}^3} + \frac{3(\boldsymbol{X}_{ji} \cdot \boldsymbol{r})\boldsymbol{X}_{ji}\boldsymbol{X}_{ji}}{X_{ji}^5} + \frac{(\boldsymbol{X}_{ji} \cdot \boldsymbol{r})\boldsymbol{I}}{X_{ji}^3}. \tag{19}$$

We now consider the time average effect of the fast oscillations by taking $\langle \boldsymbol{K}_{ji} \cdot \dot{\boldsymbol{r}} \rangle$ in (14). This involves the time average $\langle \boldsymbol{r}\dot{\boldsymbol{r}} \rangle$ and with the use of two-dimensional Cartesian coordinates $\boldsymbol{r} = (x, y) = (x_1, x_2)$ we obtain

$$\langle x_c \dot{x}_d \rangle = \tfrac{1}{2}\Gamma \varepsilon_{cd3}, \quad \Gamma \equiv \langle x\dot{y} - y\dot{x} \rangle = \langle r^2 \dot{\phi} \rangle. \tag{20}$$

The factor Γ is also twice the area swept out in the phase plane of the internal dynamics with polar coordinates (s, ϕ). Our result for the swimmer motion is

$$(\rho + \rho^{-1})\dot{\boldsymbol{X}}_j = (\rho + \rho^{-1})\boldsymbol{V} + \frac{3\varepsilon}{4}\sum_{i \neq j} \frac{\Gamma \boldsymbol{k} \times \boldsymbol{X}_{ji}}{|\boldsymbol{X}_{ji}|^3}, \tag{21}$$

where $\boldsymbol{V}$ is the swimming velocity of a single swimmer, and $\boldsymbol{k}$ is a unit vector in the z-direction. For large distances the average effect of swimmer i on swimmer j is a circulatory motion which falls off with an inverse square law.

The factor Γ can be measured from simulations, or calculated approximately in the various limits discussed in [21]. In fact provided that during the internal dynamics $s \simeq 1$ and the area is consistently swept out as one sign (so there is no cancellation in computing Γ), the speed of swimming may be approximately computed (cf. equations (3.4,3.19) of [21]) as

$$|\boldsymbol{V}| \simeq \frac{3\varepsilon}{4} \frac{\chi_2 - \chi_1}{\rho + \rho^{-1}} \Gamma. \tag{22}$$

Consistent with this, for the parameters used in the present simulations we measure

$$\Gamma \simeq 0.0393, \quad \boldsymbol{V} \simeq (-3.08, 8.01) \times 10^{-4}, \tag{23}$$

by simulating one swimmer using the internal dynamics (4,5) and measuring its motion $\boldsymbol{X}(t)$ as in [21].

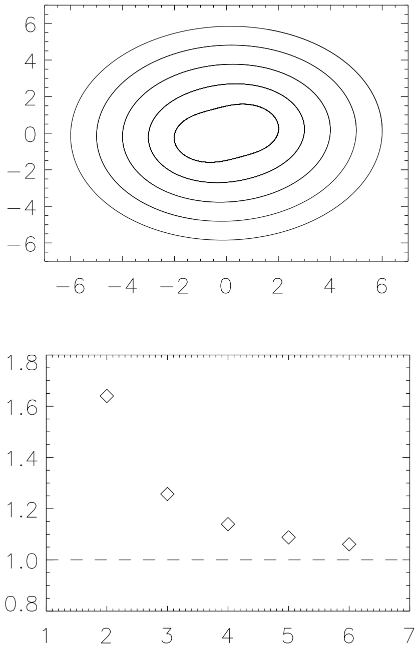

(a)

(b)

Fig. 5. (a) Relative displacement $\boldsymbol{X}_2 - \boldsymbol{X}_1$ for two swimmers with initial distance $R = 2$, 3, 4, 5 and 6. (b) Measured angular velocity $\varOmega(R)$ divided by the theoretical prediction from (24) (markers), plotted against R.

Two swimmers separated by a distance R will translate and circle each other with an angular velocity

$$\varOmega(R) = \frac{3\varepsilon}{4(\rho+\rho^{-1})}\frac{2\varGamma}{R^3}. \tag{24}$$

To confirm this we plot $\boldsymbol{X}_2 - \boldsymbol{X}_1$ in figure 5(a) which shows relative motion in a circle as a good approximation for reasonable separations. The corresponding angular velocities given in figure 5(b) show good convergence as the separation is increased. Simulations of 2–4 swimmers (not shown) with the averaged dynamics (21) give good general agreement with figure 3.

4 Passive scalar mixing

As swimmers move through the fluid they stir it: for the motions of 2–4 swimmers depicted in figure 3, we will expect to obtain a wake of stirred fluid. We investigate this numerically, looking at the qualitative behaviour. In an open system such as this, in an infinite fluid, it is natural to consider streak lines, *i.e.* the material curve produced when passive particles are emitted continuously from a point over a time interval. Such particles, with positions $\boldsymbol{x}_i(t)$, are driven by the motion of the beads that constitute the swimmers. In dimensional terms, a sphere radius R instantaneously centred at the origin moving with velocity $\boldsymbol{v}$ driven by an external force $\boldsymbol{F} = 6\pi\eta R\boldsymbol{v}$ induces a velocity for a passive particle at $\boldsymbol{x}$ of

$$\dot{\boldsymbol{x}} = \left[\frac{3R}{4s}(\hat{\boldsymbol{x}}\hat{\boldsymbol{x}}+I) - \frac{R^3}{4s^3}(3\hat{\boldsymbol{x}}\hat{\boldsymbol{x}}-I)\right]\cdot\frac{\boldsymbol{F}}{6\pi\eta R}, \quad (s\equiv|\boldsymbol{x}|\geq R) \tag{25}$$

[36] and we take $\dot{\boldsymbol{x}} = \boldsymbol{v}$ inside the sphere $x < R$ itself. For the flow field of a single swimmer, we sum the flows arising from the motion of the two beads, and in dimensionless terms replace R by $\varepsilon\rho$ for bead 1 and by ε/ρ for bead 2. (Note that for the flow field induced by the swimmer, the leading s^{-1} contributions to the flow field cancel as the forces on the two beads sum to zero.)

We now suppose we have motion of several swimmers, whose beads have positions $\boldsymbol{r}_{1j}$ and $\boldsymbol{r}_{2j}$, and velocities $\dot{\boldsymbol{r}}_{1j}$ and $\dot{\boldsymbol{r}}_{2j}$ as before, which are time stepped numerically. We specify the motion of the ith passive particle $\boldsymbol{x}_i(t)$ by

$$\begin{aligned}\dot{\boldsymbol{x}}_i =& \frac{3}{4}\sum_j\left[\frac{\varepsilon\rho}{s_{i1j}}(\hat{\boldsymbol{r}}_{i1j}\hat{\boldsymbol{r}}_{i1j}+I) - \frac{\varepsilon^3\rho^3}{4s_{i1j}^3}(3\hat{\boldsymbol{r}}_{i1j}\hat{\boldsymbol{r}}_{i1j}-I)\right]\cdot\dot{\boldsymbol{r}}_{1j}\\ &+\frac{3}{4}\sum_j\left[\frac{\varepsilon\rho^{-1}}{s_{i2j}}(\hat{\boldsymbol{r}}_{i2j}\hat{\boldsymbol{r}}_{i2j}+I) - \frac{\varepsilon^3\rho^{-3}}{4s_{i2j}^3}(3\hat{\boldsymbol{r}}_{i2j}\hat{\boldsymbol{r}}_{i2j}-I)\right]\cdot\dot{\boldsymbol{r}}_{2j}.\end{aligned} \tag{26}$$

Here $\boldsymbol{r}_{i1j} = \boldsymbol{x}_i - \boldsymbol{r}_{1j}$, $s_{i1j} = |\boldsymbol{r}_{i1j}|$, etc., with the convention that if the particle falls inside any bead, the corresponding term in the sum is replaced by the velocity of that bead. It is important to note that whereas (25) is exact for a single sphere, (26) for many is an approximation, and one that allows the particles of the streak line to penetrate beads, driven by the motion of other beads. Nonetheless we will use it and discuss the results below.

We have simulated streak lines for two and three swimmers, depicted in figure 6(a,b) and (c,d) respectively. In each case we integrated the motion of the swimmers including the full internal dynamics, over $N = 2\times10^4$ cycles of the external magnetic field. Over this time period 2×10^4 passive particles were released, from the point above the first swimmer at $(X_1(t), Y_1(t), 0) + (0, 1, 0.01)$. The point of release is thus time-dependent and is chosen to lie outside the plane in which the swimmers lie (otherwise the particles can accumulate at stable points in the two-dimensional flow restricted to this plane).

In the case of two and three swimmers, the distribution of particles about the swimmers is depicted in panels (a) and (c). There is in both cases good mixing in the vicinity of the swimmers, rather more thorough in the case of three swimmers, with some penetration of particles into the beads. In terms of mixing of the fluid on larger scales, panels (b) and (d) show a trail of scalar particles behind the swimmers, regular in the case of two swimmers, more irregular and broader for three. In both cases there is mixing of the fluid on the scale of the swimmers, in a band marking their paths through the fluid, but little penetration of the scalar particles into the region on either side.

We also investigated mixing where the swimmer beads move under the reduced dynamics given by (21); however this seemed to underestimate the amount of mixing, especially in the vicinity of the beads themselves. We conclude

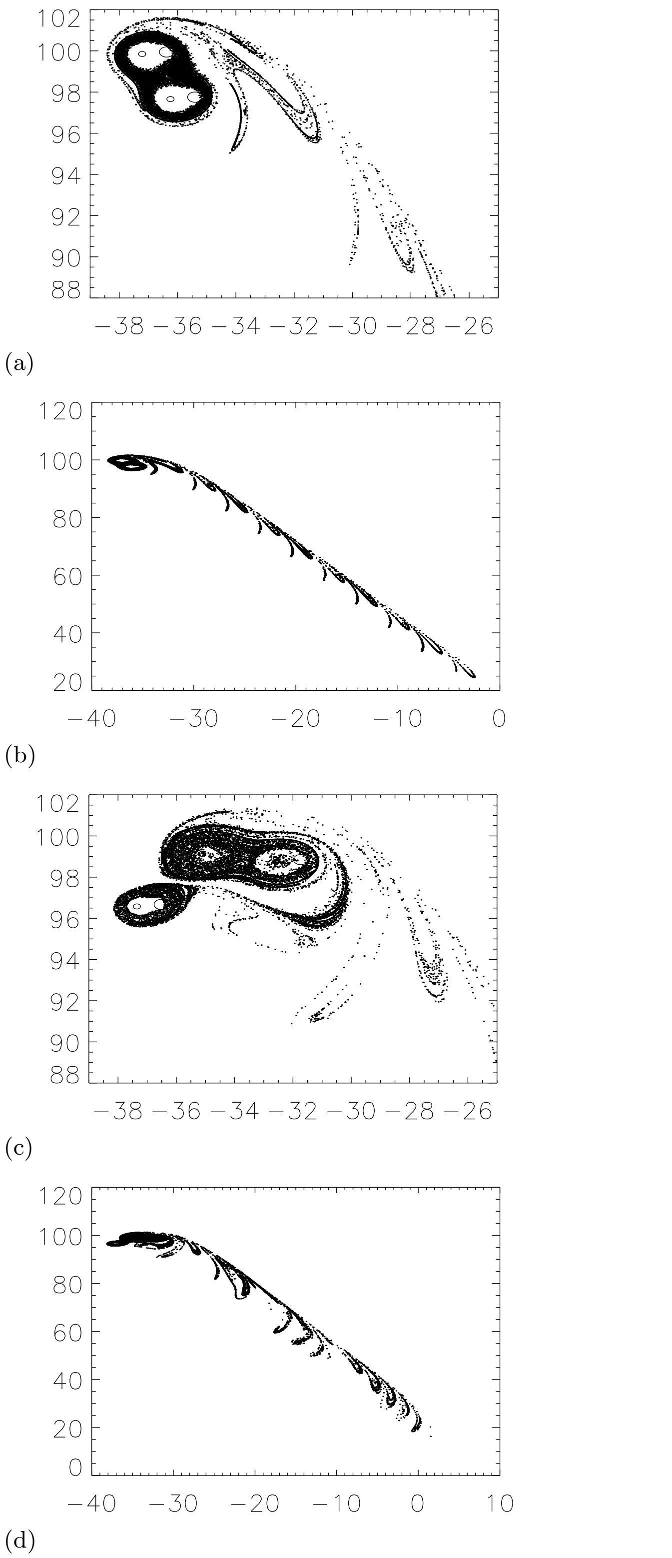

Fig. 6. Streak lines produced by the motion of (a,b) two and (c,d) three swimmers, over $N = 2 \times 10^4$ cycles. The particle distribution is shown (a,c) in the vicinity of the swimmers and (b,d) on a larger scale.

that much of the fine structure in the scalar field, including the wake, arises from the internal dynamics of the swimmers on the fast, rocking time scale, and this cannot be ignored. We have not attempted to quantify the line-stretching in the flow by measuring line length: with exponential growth, this would be too computationally expensive, particularly given the two time-scales involved in the swimmer motion.

Finally we consider briefly a regime in which the parameter A_{ext} in (8) is increased to 0.3. This increase in the external torque means that an isolated swimmer no longer shows persistent unidirectional swimming, but moves in a closed path. Two or three nearby swimmers in the fluid swim around, encircling each other. Figure 7 shows the resulting mixing for (a,b) two swimmers separated initially by (a) 3 units and (b) 4 units. In (c,d) there are three swimmers initially separated by (c) 3 and (d) 4 units. Recall that a streak line is emitted from swimmer 1 only. What we observe is that the relatively well separated swimmers in (b,d) carry around individual 'bubbles' of fluid which are well mixed by the motion on the fast time scale (excluding occasional close encounters leading to transfer of scalar as in (d)). However when the swimmers are closer together in (a,c), the bubbles merge to create a connected, well-mixed region of the fluid.

5 Discussion

We have considered the interaction of ferromagnetic driven swimmers in a viscous fluid by means of numerical simulations supported by far-field approximations. We have found an inverse square law interaction leading to circulatory motion, like a vortex in an ideal fluid but with a more rapid fall-off. This causes two swimmers to circle each other as they translate through the fluid, and three to show a braided motion. The motion of both two and three swimmers leads to Lagrangian mixing of a strip of fluid, whose width is of the order of the paths swept out by the swimmers. Note that it is the complex, driven motions of the individual swimmers that allow them to swim individually; in contrast, in the study [29] of oscillating dumb-bell swimmers it is only the interaction between two or more dumb-bells that allows their persistent motion through a viscous fluid.

It is interesting to compare our results with studies of three-sphere swimmer interactions in [27]. Each swimmer consists of 3 spheres in a line that undergo a motion that is irreversible in time. The leading effect on the fluid is an r^{-3} fall-off at long distances, supplemented by a r^{-4} fall-off that depends on the phase between the swimmers and which can be important at intermediate scales because of a larger prefactor. There is no leading order dipole contribution r^{-2} because the swimmer is invariant under simultaneous time-reversal and reversal of parity, a PT transformation. A dipole contribution would change sign and so cannot be present.

On the other hand we obtain an r^{-2} circulating, vortex-like far field about each swimmer, which also changes sign under PT transformations. Such a far field is excluded in

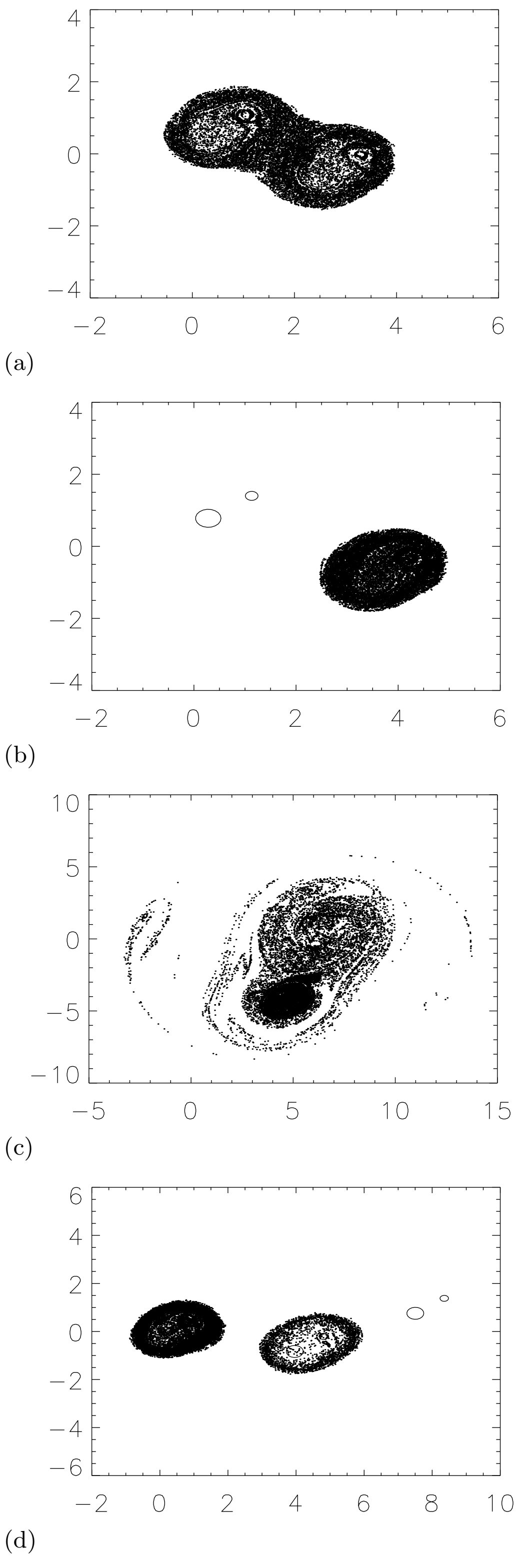

Fig. 7. Streak lines produced by the motion of (a,b) two and (c,d) three swimmers, over $N = 2 \times 10^4$ cycles with $A_{\rm ext} = 0.3$.

the 3-sphere swimmers of [27] because they have an additional reflection symmetry about their axis. The reason we obtain this dominant effect is that in a ferromagnetic microswimmer such as that modelled here, the external magnetic field driving leads to a net torque being exerted on the fluid. For a swimmer with no external assistance the constraints imposed at low Reynolds number are that the net force and net torque on the swimmer must vanish, as stressed in [25]. However the latter constraint becomes relaxed when there is external magnetic driving, and this leads to a stronger interaction between swimmers. For similar reasons, continuum models based on the interactions between populations of swimming biological organisms [37,38] may need modification for populations of magnetically driven swimmers. Other mechanisms appear to give rise to the circular swimming motions recently observed in bacteria close to a solid boundary [39] and in chemically propelled swimmers [40].

The link between the persistent swimming and the r^{-2} circulation arising from the net torque on the fluid in our swimmers is evident in equation (22) above and this indicates the generality of our results. Although there can be different swimming regimes (the distinct 'trapping' mechanisms in [21]) and we have just considered the one 'soft–hard' model, these are all associated with a net area $\frac{1}{2}\Gamma$ swept out in the internal dynamics and so with the r^{-2} circulation around the swimmer. The presence of persistent swimming is thus linked to the average fluid interactions between each of several swimmers. In short, the braiding motion of multiple swimmers, together with mixing of the fluid in between will be a general feature of magnetically driven swimmers in which net torques are exerted by swimmers on the fluid.

6 Acknowledgements

We thank M. Berger for useful discussions and for producing figure 4(a). We are grateful to J.-L. Thiffeault for discussions of mixing and swimming, and for sending us papers in advance of publication.

References

1. Lighthill. M.J. 1969 *Ann. Rev. Fluid Mech.* **1**, 413–446.
2. Childress. S. 1981 *Mechanics of swimming and flying.* Cambridge University Press.
3. Maxworthy, T. 1981 *Ann. Rev. Fluid Mech.* **13**, 329–350.
4. Triantafyllou, M.S., Triantafyllou, G.S. & Yue, D.K.P. 2000 *Ann. Rev. Fluid Mech.* **32**, 33–53.
5. Wang, Z.J. 2005. *Ann. Rev. Fluid Mech.* **37**, 183–210.
6. Najafi, A. & Golestanian, R. 2004 *Phys. Rev. E* **69**, 062901.
7. Earl, D.J., Pooley, C.M., Ryder, J.F., Bredberg, I. & Yeomans, J.M. 2007 *J. Chem. Phys.* **126**, 064703.
8. Golestanian, R. & Ajdari, A. 2008 *Phys. Rev. E* **77**, 036308.
9. Biswal S.L., Gast A.P. 2004 *Anal Chem.* **76**. 6448–55.
10. Dreyfus, R., Baudry, J., Roper, M.L., Fermigier, M., Stone, H.A. & Bibette, J. 2005 *Nature* **437**, 04090.
11. Cēbers, A. & Javaitis, I. 2004 *Phys. Rev. E* **69**, 021404.

12. Gauger, E. & Stark, H. 2006 *Phys. Rev. E* **74**, 021907.
13. Keaveny, E.E. & Maxey, M.R. 2008 *J. Fluid Mech.* **598**, 293–319.
14. Tierno, P., Golestanian, R., Pagonabarraga, I. & Sagues, F. 2008 *Phys. Rev. Lett.*, **101**, 218304.
15. Shields, A.R., Fiser, B.L., Evans, B.A., Falvo, M.R., Washburn, S. & Superfine, R. 2010 *Proc. Nat. Acad. Sci.* **107**, 15670–15675.
16. Vilfan, M., Potocnik, A., Kavcic, B., Osterman, N., Poberaj, I., Vilfan, A. & Babic, D. 2010 *Proc. Nat. Acad. Sci.* **107**, 1844-1847.
17. Coq, N., Bricard, A., Delapierre, F.-D., Malaquin, L., du Roure, O., Fermigier, M. & Bartolo, D. 2011 *Phys. Rev. Lett.* **107**, 014501.
18. Ogrin, F.Y., Petrov, P.G. & Winlove, C.P. 2008 *Phys. Rev. Lett.* **100**, 218102.
19. Vilfan, A. & Stark, H. 2009 *Phys. Rev. Lett.* **103**, 199801.
20. Ogrin, F.Y., Petrov, P.G. & Winlove, C.P. 2009 *Phys. Rev. Lett.* **103**, 199802.
21. Gilbert, A.D., Ogrin, F.Y., Petrov, P.G. & Winlove, C.P. 2011 *QJMAM*, **64**, 239–263.
22. Purcell, E.M. 1977 *Am. J. Phys.* **45**, 3–11.
23. Felderholf, B.U. 2006 *Phys. Fluids* **18**, 063101.
24. Friedman, G. 2007 *Phys. Fluids* **19**, 079101.
25. Felderholf, B.U. 2007 *Phys. Fluids* **19**, 079102.
26. Falcucci, G., Chiatti, G., Succi, S., Mohamad, A. A. & Kuzmin, A. 2009 *Phys. Rev. E* **79**, 056706.
27. Pooley, C.M., Alexander, G.P. & Yeomans, J.M. 2007 *Phys. Rev. Lett* **99**. 228103.
28. Alexander, G.P., Pooley, C.M. & Yeomans, J.M. 2008 *Phys. Rev. E* **78**, 045302.
29. Alexander, G.P. & Yeomans, J.M. 2008 *EPL* **83**, 34006.
30. Alexander, G.P., Pooley, C.M. & Yeomans, J.M. 2009 *J. Phys.: Condens. Matter* **21**, 204108.
31. Putz, V.B. & Yeomans, J.M. 2009 *J. Stat. Phys.* **137**, 1001–1013.
32. Alexander, G.P. & Yeomans, J.M. 2010 *Exp. Mech.* **50**, 1283–1292.
33. Happel, J. & Brenner, H. 1983 *Low Reynolds number hydrodynamics*. Kluwer, Dordrecht.
34. Boyland, P.L., Aref, H. & Stremler, M.A. 2000 *J. Fluid Mech.* **403**, 277–304.
35. Thiffeault, J.-L. 2010 *Chaos*, **20**, 017516.
36. Landau, L.D. & Lifshitz, E.M. 1959 *Fluid mechanics*. Butterworth–Heinemann.
37. Saintillian, D. & Shelley, M.J. 2008 *Phys. Fluids* **20**, 123304.
38. Ishikawa, T. & Pedley, T.J. 2008 *Phys. Rev. Lett.* **100**, 088103.
39. Lauga, E., DiLuzio, W.R., Whitesides, G.M. & Stone, H.A. 2006 *Biophys. J.* **90**, 400–412.
40. Ebbens, S., Jones, R.A.L., Ryan, A.J., Golestanian, R., Howse, J.R. 2010 *Phys. Rev. E* **82**, 015304.